

A Skew Dividing Surface for Accurate Nonadiabatic Mean-Field Ring Polymer Rates

Britta A. Johnson¹ and Nandini Ananth^{1, a)}

Department of Chemistry and Biochemistry, Cornell University, Ithaca, New York 14850 U.S.A

(Dated: 29 April 2021)

Mean-Field Ring Polymer Molecular Dynamics (MF-RPMD) is a powerful, efficient, and accurate method for approximate quantum dynamic simulations of multi-level system dynamics. Initial efforts to compute nonadiabatic reaction rates using MF-RPMD were not successful; recent work showed that this can be remedied by including a simple, if *ad hoc*, correction term that accounts for the formation of ‘kinked’ or mixed electronic state ring polymer configurations. Here, we build on this idea, introducing a electronic state population based reaction coordinate and novel skew dividing surface that constrains nuclear positions to configurations where the reactant and product state potentials are near-degenerate *and* that samples kinked electronic state configurations. We then demonstrate the numerical accuracy of this method in computing rates for a series of nonadiabatic model systems.

I. INTRODUCTION

Nonadiabatic condensed phase reactions play a critical role in understanding reaction mechanisms for a diverse range of interesting systems; these reactions range from proton coupled electron transfer in biological systems to charge transfer and fluorescence in energetic materials.^{1–6} The development of accurate and scalable theoretical methods for characterizing nonadiabatic energy and charge transfer remains an outstanding challenge.

The Marcus electron transfer rate is perhaps the most popular of the nonadiabatic rate theories, but it is limited by the assumption of parabolic potentials and a classical solvent.⁷ The Wolynes rate theory correctly incorporates nuclear quantum effects by using path integral Monte Carlo methods to compute Fermi Golden Rule rates.⁸ Despite its many successes,⁹ this theory does not yield the correct classical rates for high-temperature anharmonic systems. This failure was remedied by a recently introduced Golden-Rule Quantum Transition State (GR-QTST)^{10–12} rate theory developed based on insights drawn from semiclassical^{13–15} and ring polymer instanton theories.^{16–19} Finally, the Linear Golden-Rule approximation for nonadiabatic rates was introduced to address the size inconsistencies observed in GR-QTST simulations of condensed phase systems.^{20,21} These rate theories are accurate and efficient but are limited to the golden-rule weak coupling limit. In addition, while rate theories play a key role in understanding and interpreting experimental studies, and can even provide insights into the dominant paths (instantons), the need for detailed mechanistic insights drives the development of direct dynamic methods for rate calculations.

A range of real-time dynamic methods including mixed quantum-classical^{22–25} and semiclassical methods^{26–35} have been used to simulate nonadiabatic reaction dynamics and compute rates; however, many of these

methods cannot be easily scaled to the simulation of large condensed phase reactions. Path integral based methods like centroid-molecular dynamics^{36,37} and ring polymer molecular dynamics (RPMD)³⁸ have shown particular promise in modeling condensed phase energy transfer reactions.^{39–45} These methods capture nuclear quantum effects like tunneling and zero-point energy while using only classical trajectories making them suitable for atomistic simulations of charge transfer in condensed phase systems. In particular, ring polymer molecular dynamics has been used to accurately calculate thermal rate constants for electron transfer (ET) in the normal and activationless regimes, and proton-coupled electron transfer.^{46–48} RPMD has also been extended to systems with coupled electronic states with the more successful formulations including mean-field (MF)-RPMD,⁴⁹ kinetically constrained (KC)-RPMD,^{50–52} nonadiabatic RPMD,⁵³ coherent-state RPMD,⁵⁴ and mapping-variable RPMD.^{55–58} KC-RPMD has been previously used to compute reaction rates for a model ET system in the normal and inverted Marcus regimes. Further, ring polymer surface hopping methods have been developed to add nuclear quantum effects to nonadiabatic surface hopping simulations; these methods work well for model systems despite the fact that the dynamics do not conserve the quantum Boltzmann distribution.^{59–62} Of the multi-state RPMD methods, MF-RPMD is uniquely efficient, relying on effective state-averaged electronic forces to drive nuclear dynamics and requiring no additional variables making it suitable for large scale atomistic simulations.

Initial efforts to compute nonadiabatic reaction rates from MF-RPMD significantly overestimated the rate.^{51,63,64} Previously, one of us showed that this could be remedied by ensuring MF-RPMD trajectories sample ‘kinked’ or mixed-electronic state ring polymer configurations at the dividing surface.⁶⁴ Unfortunately, the *ad hoc* introduction of an additional constraint on the types of electronic state configurations sampled resulted in an inconsistent flux-side expression for the rate constant and a difficult-to-implement simulation protocol. Here, we

^{a)}ananth@cornell.edu

present a rate expression that is obtained using a novel skew dividing surface and an electronic population-based reaction coordinate for the computation of nonadiabatic rates. We demonstrate the accuracy of this approach in a series of numerical simulations on model nonadiabatic ET systems over a wide range of driving forces.

This paper is organized as follows. In Section II we briefly review the MF-RPMD formalism, and introduce the new skew reaction coordinate. In section III we describe the model systems studied here and section IV outlines the details of the rate calculation. In section V we numerically demonstrate sampling by the skew coordinate and present the results of our nonadiabatic rate calculations. We summarize our findings in section VI.

II. THEORY

A. Mean-Field Ring Polymer Molecular Dynamics

In this section we review MF-RPMD⁶⁴. For a general K -level system with d nuclear degrees of freedom, the diabatic Hamiltonian is

$$\hat{H} = \sum_{j=1}^d \frac{\hat{P}_j^2}{2M_j} + \sum_{n,m=1}^K |n\rangle V_{nm}(\hat{R}) \langle m|, \quad (1)$$

where \hat{R} and \hat{P} are d -dimensional nuclear position and momentum vector operators, respectively. The quantum partition function is discretized via repeated insertion of N copies of the identity to obtain

$$Z = \text{Tr}[e^{-\beta\hat{H}}] = \int d\{R_\alpha\} \sum_{\{n_\alpha\}=1}^K \prod_{\alpha=1}^N \langle R_\alpha, n_\alpha | e^{-\beta_N \hat{H}} | R_{\alpha+1}, n_{\alpha+1} \rangle, \quad (2)$$

where $\beta_N = 1/(Nk_B T)$, T is temperature, N is the number of imaginary time slices (or beads), and R_α, n_α refer to the nuclear position and electronic state of the α^{th} bead, respectively. In Eq. 2, we use a shorthand for the multi-dimensional integral over nuclear coordinates and summation over electronic states, $\int d\{R_\alpha\} = \int dR_1 \int dR_2 \dots \int dR_N$ and $\sum_{\{n_\alpha\}=1}^K = \sum_{n_1} \sum_{n_2} \dots \sum_{n_N}$. Evaluating the matrix elements using the Trotter and short-time approximations, we obtain,^{65,66}

$$Z \propto \lim_{N \rightarrow \infty} \int \{dR_\alpha\} e^{-\beta_N V_N(\{R_\alpha\})} \text{Tr}[\Gamma], \quad (3)$$

where

$$V_N = \sum_{j=1}^d \sum_{\alpha=1}^N \left[\frac{M_j}{2\beta_N^2} (R_{j,\alpha} - R_{j,\alpha+1})^2 \right], \quad (4)$$

$$\Gamma = \prod_{\alpha=1}^N M(R_\alpha), \quad (5)$$

and M is the $K \times K$ -dimensional matrix

$$M_{nm}(R_\alpha) = \begin{cases} e^{-\beta_N V_{nn}(R_\alpha)} & n = m \\ \beta_N V_{nm}(R_\alpha) e^{-\beta_N V_{nn}(R_\alpha)} & n \neq m \end{cases} \quad (6)$$

Finally, moving the trace in Eq. 3 into the exponential and introducing N normalized Gaussian integrals in nuclear momenta, we obtain a phase-space expression for the canonical partition function,

$$Z \propto \lim_{N \rightarrow \infty} \int \{dR_\alpha\} \int \{dP_\alpha\} e^{-\beta_N H_N(\{R_\alpha\}, \{P_\alpha\})}, \quad (7)$$

where the MF-RPMD Hamiltonian is

$$H_N = \sum_{j=1}^d \sum_{\alpha=1}^N \left[\frac{M_j}{2\beta_N^2} (R_{j,\alpha} - R_{j,\alpha+1})^2 + \frac{P_{j,\alpha}^2}{2M_j} \right] - \frac{1}{\beta_N} \ln(\text{Tr}[\Gamma]). \quad (8)$$

The MF-RPMD approximation to quantum real-time thermal correlation functions is obtained by sampling initial conditions from an exact quantum canonical ensemble and time-evolving trajectories under the MF-RPMD Hamiltonian in Eq. 8 with M_j chosen to the physical mass of the nuclei.

B. A Skew Dividing Surface

For a general reaction with a barrier, the rate constant can be written in terms of a flux-side correlation function^{65,67}.

$$k = \lim_{t \rightarrow \infty} \frac{\langle \delta(\xi_0 - \xi^\ddagger) \dot{\xi}_0 h(\xi_t - \xi^\ddagger) \rangle}{\langle h(\xi^\ddagger - \xi_0) \rangle}, \quad (9)$$

where the angular brackets indicate a canonical ensemble average, δ is a delta function, and h is the Heaviside function. For a K -level system, the generalized reaction coordinate, ξ , may be a function of the nuclear $\{R\}$ and electronic state $\{n\}$ variables; ξ_0 is the initial value of this coordinate at time $t = 0$, ξ_t is the value at time t , and ξ^\ddagger is value at the dividing surface.

The MF-RPMD Hamiltonian in Eq. 8 is an explicit function of the nuclear positions and momenta, with the effective mean-field potential, Γ , obtained by tracing over all possible electronic state configurations. Previous attempts to calculate nonadiabatic reaction rates using MF-RPMD relied on a nuclear centroid based definition of the dividing surface, $\delta(\bar{R} - R^\ddagger)$, where the reaction coordinate is the centroid, $\bar{R} = \frac{1}{N} \sum_\alpha R_\alpha$, and R^\ddagger represents the nuclear configuration at which the two diabatic electronic state potentials cross. It was shown that MF-RPMD rates computed with this centroid based reaction coordinate were accurate for adiabatic systems, but significantly overestimated the rate for nonadiabatic systems.^{50,63} One of us previously showed that the low probability of sampling ‘kinked’ or multi-electronic state

ring polymer configurations for nonadiabatic processes, even at the nuclear centroid dividing surface, was responsible for the failure of MF-RPMD.⁶⁴ Further, it was established that a dividing surface obtained by sampling only kinked configurations *and* constraining the nuclear centroid position resulted in accurate MF-RPMD rates for a range of nonadiabatic model systems.⁶⁴ However, the mismatch between reaction coordinate and the *ad hoc* doubly constrained dividing surface resulted in an inconsistent flux-side correlation function that was challenging to implement in both the normal and inverted Marcus regimes. Here, we propose an improved MF-RPMD rate expression by introducing a new ‘skew’ dividing surface and population-based reaction coordinate. We show the skew dividing surface ensures that the reaction bottleneck is described by kinked ring polymer configurations in the vicinity of R^\ddagger without any additional constraints.

We start by recognizing that the electronic force on the nuclear degrees of freedom in MF-RPMD is due to the mean-field potential, $\Gamma(\{R_\alpha\})$ in Eq. 5, an average over all possible electronic state configurations. Because we no longer have explicit electronic state information, reaction coordinates, like the centroid coordinate, that work well for single surface reactions cannot be used to describe the progress of a reaction where the reactant and product correspond to distinct electronic states. Here, we introduce a coordinate that can distinguish between different electronic state configurations and that uses the relative population changes to track the progress of the reaction,

$$\Delta P = \text{Tr}[\Gamma_0] - \text{Tr}[\Gamma_N], \quad (10)$$

where

$$\Gamma_k = \prod_{\alpha=1}^{N-k} [M(R_\alpha)\mathbb{P}_2] \prod_{\alpha=N-k+1}^N [M(R_\alpha)\mathbb{P}_1], \quad (11)$$

and \mathbb{P}_i is the projection operator corresponding to the i^{th} electronic state. Physically, Eq. 11 is representative of MF-RP configurations where k beads are in electronic state 1 and the remaining $N - k$ beads are in state 2. This reaction coordinate, $\Delta P(\{R_\alpha\})$, like the centroid coordinate, is a function of nuclear bead positions but unlike the centroid coordinate can distinguish between a system in the reactant electronic state and product electronic state; ΔP moves from being negative in the reactant region to positive in the product region.

In keeping with a reaction that involves a change in electronic state, the dividing surface is defined by MF-RP configurations sampled on a subset of kinked or mixed electronic-state potentials. Constraining the system to this dividing surface is then achieved by sampling nuclear configurations on $\text{Tr}[\Gamma_{N^\ddagger}]$ where $0 < k < N$. Values of N^\ddagger depend on the driving force; as the driving force increases, N^\ddagger also increases as shown in the cartoon Fig. 1. We note that this idea is in keeping with studies of the MF-RP instanton for multistate systems that has an increasing number of RP beads in the reactant state as we

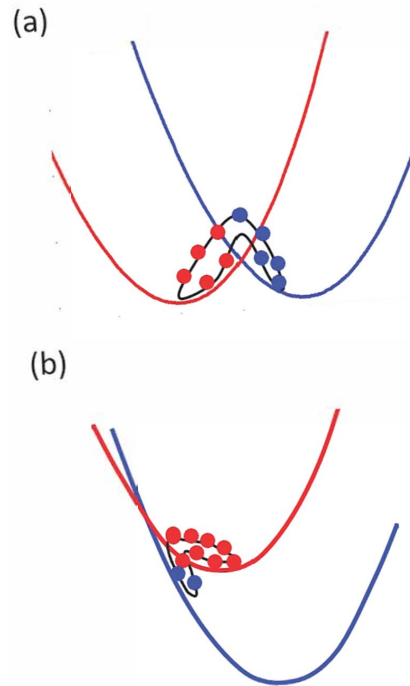


FIG. 1. (a) Shows a symmetric two-level system where half the RP beads are in the reactant state (red) and the other half are in the product state (blue). As the reactant state is destabilized and the driving force increases, we find that constraining nuclear RP configurations to the vicinity of the diabatic crossing can be achieved by increasing the number of beads in the reactant state as shown in (b).

increase the driving force in the Marcus normal regime.⁶⁸ Formally, the calculated rate will be independent of the choice of N^\ddagger , however, certain choices can make the simulation numerically unfeasible.

To find ‘good’ N^\ddagger values, we generate histograms of the nuclear configurations sampled from the kinked MF-RP potential, $\text{Tr}[\Gamma_{N^\ddagger}^\ddagger]$. For simple system-bath models, we find that N^\ddagger values with distributions centered around the nuclear configurations at which the two diabatic potentials cross perform the best. This can be easily understood: when we sample nuclear configurations away from the crossing, in particular towards the reactant minimum, there is a large barrier to the centroid reaching the crossing, making this a rare event and one that is unlikely to be sampled by dynamics on a reasonable timescale. This rare event problem is well understood and one that is best avoided by a good choice of N^\ddagger . As we demonstrate, for the models considered here, and we expect for more general model systems, it is not challenging to identify a range of suitable N^\ddagger values.

Using our new reaction coordinate and dividing surface definitions, we obtain an expression for the rate defined

as the long-time limit of a flux-side correlation function,

$$k = \lim_{t \rightarrow \infty} \frac{\int d\{R_\alpha, P_\alpha\} e^{-\beta_N H_N^0} \text{Tr}[\Gamma_{N^\ddagger}] \Delta \dot{P}(0) h(\Delta P(t))}{\int d\{R_\alpha, P_\alpha\} e^{-\beta_N H_N^0} \text{Tr}[\Gamma_N(0)]}, \quad (12)$$

where H_N^0 is the free ring polymer Hamiltonian that includes only terms on the first line of Eq. 8

C. Nonadiabatic Rate Theories

The Marcus theory (MT) rate for a nonadiabatic electron transfer reaction with a classical solvent is,⁶⁹

$$k_{\text{MT}} = \frac{2\pi}{\hbar} |V_{nm}|^2 \sqrt{\frac{\beta}{4\pi\lambda}} e^{-\beta(\lambda-\epsilon)^2/4\lambda}, \quad (13)$$

where λ is the reorganization energy, ϵ is the driving force, and V_{nm} is the diabatic coupling between the reactant and product electronic states.

Fermi's golden rule rate theory for a nonadiabatic electron transfer system where the reactant and product state potential energy surfaces are displaced harmonic oscillators with frequency ω_s and with a quantized solvent take the simple analytical form^{70,71}

$$k_{\text{FGR}} = \frac{2\pi}{\hbar\omega_s} |\Delta|^2 e^{vz-S \coth(z)} I_v(S \text{csch}(z)), \quad (14)$$

where $z = \beta\omega_s/2$, $v = \epsilon/\omega_s$, $S = M_s\omega_s V_d^2/2\hbar$, M_s is the solvent mass, I_v is a modified Bessel function of the first kind, and V_d is the horizontal displacement of the diabatic potential energy surfaces.

III. MODEL SYSTEM

We calculate the rates for a model condensed-phase ET system with a potential

$$V(\hat{R}) = V_S(\hat{s}) + V_B(\hat{R}) \quad (15)$$

where the configuration vector $\hat{R} = \{\hat{s}, \hat{Q}\}$ represents the solvent polarization coordinate, s , and the bath coordinates, Q . The diabatic potential energy matrix is

$$V_S(\hat{s}) = \begin{pmatrix} V_{11}(\hat{s}) & \Delta \\ \Delta & V_{22}(\hat{s}) \end{pmatrix}, \quad (16)$$

where the diagonal elements are $V_{11}(\hat{s}) = A\hat{s}^2 + B\hat{s} + \epsilon$, $V_{22}(\hat{s}) = A\hat{s}^2 - B\hat{s}$, the driving force is represented by ϵ , and the diabatic coupling a constant, Δ . The solvent coordinate is linearly coupled to a thermal bath of f harmonic oscillators,

$$V_B(\hat{R}) = \sum_{j=1}^f \left[\frac{1}{2} M_B \omega_j^2 \left(\hat{Q}_j - \frac{c_j \hat{s}}{M_B \omega_j^2} \right)^2 \right] \quad (17)$$

| Parameters | Value |
|--------------------|------------------------|
| A | 4.772×10^{-3} |
| B | 2.288×10^{-2} |
| ϵ | 0.0 – 0.2366 |
| Δ | 6.69×10^{-7} |
| M_S | 1836.0 |
| M_B | 1836.0 |
| f | 12 |
| ω_c | 2.28×10^{-3} |
| $\eta/M_B\omega_c$ | 1.0 |
| T | 300 K |

TABLE I. ET model parameters given in atomic units unless otherwise indicated.

where M_S and M_B are the solvent and bath mass respectively. The bath is described by an Ohmic spectral density

$$J(\omega) = \eta\omega e^{-\frac{\omega}{\omega_c}} \quad (18)$$

where ω_c is the cutoff frequency and η is the dimensionless friction coefficient. The spectral density is discretized into f oscillators³⁹

$$\omega_j = -\omega_c \ln \left(\frac{j-0.5}{f} \right) \quad (19)$$

with coupled strengths

$$c_j = \omega_j \left(\frac{2\eta M_B \omega_c}{f\pi} \right)^{1/2} \quad (20)$$

The ET model parameters are shown in Table I.

IV. SIMULATION DETAILS

The rate expression in Eq. 21 may still be challenging to implement since the numerator requires sampling an ensemble constrained to our skew dividing surface while the denominator requires efficient sampling of the reactant region. To ensure proper sampling of all important regions of configuration space, we introduce an identity in the form of an integral over all possible nuclear RP centroid configurations to obtain

$$k = \lim_{t \rightarrow \infty} \frac{\int ds' \langle \Gamma_{N^\ddagger} \Delta \dot{P}(0) h(\Delta P(t)) \rangle_w}{\int ds' \langle \Gamma_N \rangle_w} \quad (21)$$

where $\langle \dots \rangle_w$ is used to indicate a phase space ensemble average over the nuclear bead configurations obtained by importance sampling from the distribution

$$w = e^{-\beta_N H_N^0(\{R_\alpha, P_\alpha\})} \delta(\bar{s} - s'). \quad (22)$$

The numerator and denominator are evaluated using a standard Metropolis algorithm to sample free RP configurations from $e^{-\beta_N H_N^0(\{R_\alpha, P_\alpha\})}$ in each window. We

then impose the constraint by shifting the solvent RP centroid to \bar{s} to the s' value associated with each window. By scrolling through all possible nuclear RP centroid configurations, we ensure that the numerator and the denominator are sampled adequately. The integral over s' is evaluated using the trapezoid rule.

We establish the mean-field path integral converges with $N = 32$ beads for all simulations presented here. Importance sampling is performed in each window using 11000 decorrelated Monte Carlo steps, and the final 10000 configurations are used as initial conditions for trajectories evolved under the MF-RPMD Hamiltonian in equation 8 with a timestep of 0.05 a.u. The average initial velocity, $\Delta P(0)$ is obtained by averaging over the finite difference derivative of ΔP calculated for three small intervals of time, $\Delta t = 5, 7, 10$ a.u. The integral over the solvent centroid configurations is performed over 150 windows evenly spaced between $s = -4.5$ and $s = +1.5$ for Models I-VIII. Model IX simulations are performed with 150 evenly spaced points between $s = -6.5$ and $s = -0.5$.

1. A Modified Implementation in the Inverted Regime

Physically, the probability of forming kinked configurations, where neighboring beads of the ring polymer are in different electronic states, depends on both the magnitude of the off-diagonal diabatic coupling and the energy gap between the reactant and product states. In the normal regime, we find that the kink probabilities computed using the MF-RP potential, $\Gamma(\{R_\alpha\})$ in Eq. 5 with the interaction matrix defined in Eq. 6, do indeed show a decreased probability at nuclear configurations where the energetic gap between reactant and product states is large. However, in the inverted regime, we see a breakdown of this: specifically, we find that in regions where the product state is much more favorable than the reactant state, the Boltzmann weight of beads in the product state is numerically larger than the penalty associated with kink formation, resulting in an unphysically large probability of kink formation in regions where the reactant and product are energetically very different.

We correct for this by a simple modification of the nuclear interaction matrix in Eq. 6 that is used in computing Γ_N^\ddagger . Specifically, we replace V_{22} by $V_{11} + |V_{22} - V_{11}|$ in the appropriate off-diagonal term of the interaction matrix. This ensures that the energetic penalty associated with kink formation is correctly captured, since the value now depends only on the magnitude of the energy gap between states. Note that this is only used in the calculation of Γ_{N^\ddagger} ; dynamics are performed using the MF-RPMD Hamiltonian and the remaining terms in Eq. 21 are unaffected by this change.

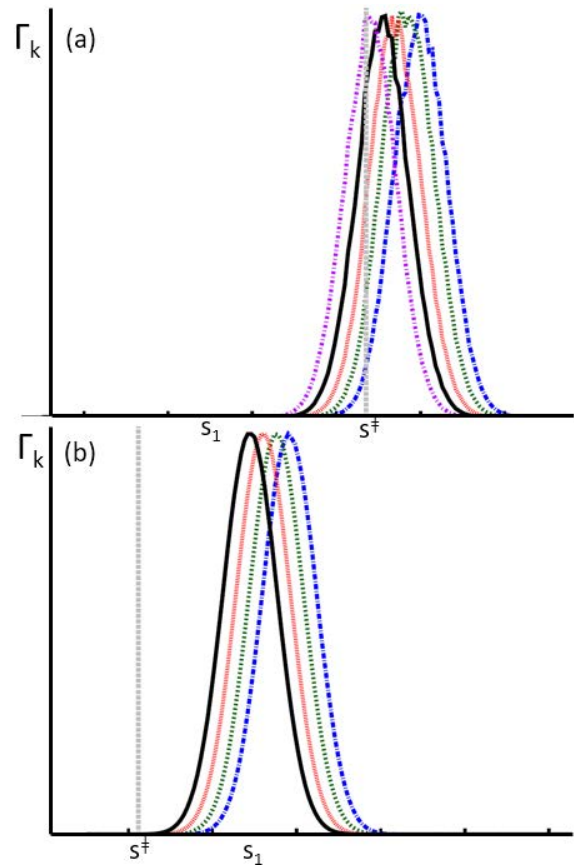


FIG. 2. Plots of the Γ_k functions for (a) model III and (b) model VIII. In both figures, the location of the diabatic crossing is designated by a dotted line at s^\ddagger , the reactant minimum indicated by s_1 , and Γ_k with $k = N^\ddagger$ is plotted as a black solid line. (a) For model III, Γ_k with $k = 16$ is shown in blue, $k = 17$ is in dark green, $k = 18$ is in red, $k = 19$ is in black, and $k = 20$ is in magenta. (b) For model VIII, Γ_k with $k = 28$ is shown in blue, $k = 29$ in dark green, $k = 30$ in red, and $k = 31$ in black.

V. RESULTS AND DISCUSSION

We present the results of our rate calculations for nine model systems that differ only in the driving force, ε , values; six of these systems (Models I-VI) are located in the normal regime and three (Models VII-IX) are in the inverted regime. To select the N^\ddagger values for each model, we look at the values for $\Gamma_k(\{R_\alpha\})$ for individual beads as a function of nuclear position.

Figure 2 shows a sample of the Γ_k curves for a model in the normal regime (Models III) and one inverted regime model (Model VIII). For each model, we find that there is a range of k values where Γ_k is maximized near the crossing (denoted s^\ddagger in the figure), the point where the reactant and product state are degenerate. We note that the inverted regime Γ_k is modified as described in the simulation details; we find that $N^\ddagger = 31$ is necessary to ensure that the dividing surface includes nuclear configurations to the left of the reactant minimum towards the

diabatic crossing. For each model in the normal regime, we select an N^\ddagger value such that Γ_{N^\ddagger} peaks close to the crossing; the specific values we use are listed in Table II.

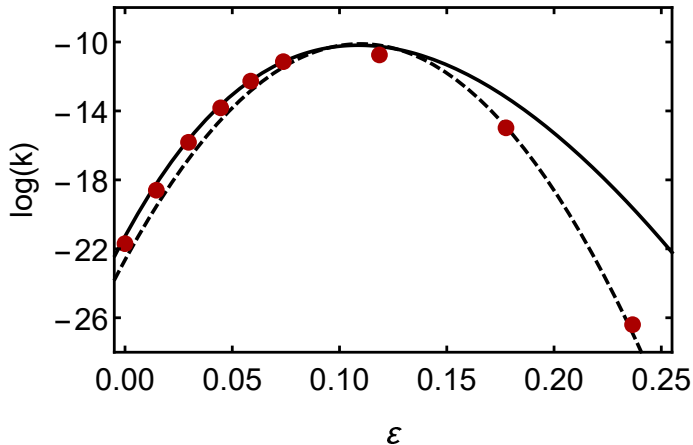


FIG. 3. ET rates for models I-IX. MF-RPMD rates with the skew reaction coordinate are shown as red circles, error bars are within the symbol size. The Fermi's Golden rule rates lie along the solid black line and the Marcus theory rates lie along the dashed line

We present the MF-RPMD rate results in Fig. 3 and tabulate the corresponding values in Table II. We find that the new reaction coordinate performs remarkably well in the normal regime, yielding results that are in quantitative agreement with Fermi Golden Rule rates for all six model systems. In the inverted regime, we find good agreement with Marcus theory rates rather than the golden rule rates. This initially surprising result can be attributed to the nature of our approximate MF-RPMD dynamics. Decomposing contributions to the reaction rate from different nuclear configurations, we find that the dominant contribution is at the crossing. At nuclear configurations where one may reasonably expect tunneling effects to allow for a non-zero rate contribution, we find that the Boltzmann-weighted MF-RPMD dynamics lead to very small values of velocity, $\Delta P \approx 0$. In order to obtain FGR rates, then, it is likely we will need to move beyond MF-RPMD dynamics.

For four model systems (I and III in the normal regime, and VII and IX in the inverted regime) we show, in Table III, the range of N^\ddagger values for which the rate is relatively unchanged. In the normal regime, for large N^\ddagger values, we find that the dynamic trajectories do not scale the energetic barrier necessary to reach the crossing in the timescale of the simulation. In the inverted regime, we have a different problem: small N^\ddagger values, corresponding to a large number of beads in the product state, result in an initial distribution of nuclear configurations far from the crossing (indeed, typically we see distributions that peak at configurations between reactant and product minima). Since our dynamics are classical, MF-RPMD trajectories initialized to such configurations do not pass through the reaction bottleneck yielding rates

| Model | ε | N^\ddagger | $\log(k_{\text{MT}})$ | $\log(k_{\text{MF}})$ | $\log(k_{\text{FGR}})$ |
|-------|---------------|--------------|-----------------------|-----------------------|------------------------|
| I | 0.00 | 16 | -22.65 | -21.7 | -21.28 |
| II | 0.0146 | 17 | -19.53 | -18.6 | -18.23 |
| III | 0.0296 | 19 | -16.79 | -15.82 | -15.66 |
| IV | 0.0446 | 21 | -14.52 | -13.82 | -13.65 |
| V | 0.0586 | 23 | -12.83 | -12.27 | -12.23 |
| VI | 0.0738 | 25 | -11.45 | -11.14 | -11.15 |
| VII | 0.1186 | 29 | -10.19 | -10.75 | -10.26 |
| VIII | 0.1776 | 31 | -14.91 | -14.98 | -13.20 |
| IX | 0.2366 | 31 | -26.89 | -26.4 | -19.63 |

TABLE II. ET rates for a range of driving forces. We report the N^\ddagger value used for each model, the corresponding Marcus theory rates (k_{MT}), MF-RPMD rates (k_{MF}), and Fermi Golden Rule rates (k_{FGR}) for each model. We see that the MF-RPMD rates are in near-perfect agreement with FGR rates in the normal regime and agree equally well with MT rates in the inverted regimes. All rate constants are in atomic units

that are significantly higher than expected.

| Model | N^\ddagger range | $\log(\bar{k})$ | σ_k | k_{FGR} |
|-------|--------------------|-----------------|------------|------------------|
| I | 1-21 | -21.63 | 0.3 | -21.28 |
| I | 11-20 | -21.45 | 0.2 | -21.28 |
| III | 1-21 | -15.46 | 0.3 | -15.66 |
| III | 17-21 | -15.61 | 0.3 | -15.66 |
| VII | 27-31 | -10.39 | 0.3 | -10.26 |
| IX | 29-31 | -26.01 | 0.1 | -19.63 |

TABLE III. The rates for models I, III, VII, and IX are computed by averaging over a specific range of N^\ddagger values. The reported log average rate, $\log(\bar{k})$, and standard deviation, σ_k , indicate the relative robustness of our rate with respect to a subset of N^\ddagger choices. The options are considerably smaller in the inverted regime where a large number of beads on state 1 are required to ensure that we are not primarily sampling nuclear configurations at the reactant minimum. All rate constants are in atomic units

VI. CONCLUSION

We demonstrate that the skew dividing surface and population-based reaction coordinate introduced here can be used to obtain a rigorous MF-RPMD rate theory that is quantitatively accurate for the computation of nonadiabatic reaction rates in a wide range of model systems. While we do not compute rates for the adiabatic regime here, we do note that we have previously demonstrated that for model 1, with $N^\ddagger = 16$, we are able to recover Kramer's rate theory rates for adiabatic reactions⁶⁴. Future studies will include quantifying the accuracy of our approach over a wider range of models including different friction regimes, temperatures, systems that exhibit multiple transitions states as well as regions

of extended electronic coupling.

MF-RPMD is the most efficient and easy to implement of the RPMD-based methods developed to simulate multi-state system dynamics, and we have shown that the use of a skew dividing surface enables the simulation of nonadiabatic processes. The form of our dividing surface requires only knowledge of the driving force regime for a particular reaction (information that is typically known even for complex systems), placing atomistic simulations of nonadiabatic reactions in the condensed phase within reach.

VII. ACKNOWLEDGEMENTS

The authors would like to acknowledge Prof. Greg Ezra for helpful discussion and thank the reviewers of this paper for insightful comments. This work was primarily supported by the U.S. Department of Energy, Office of Basic Energy Sciences, Division of Chemical Sciences, Geosciences and Biosciences through the Nanoporous Materials Genome Center under award numbers DE-FG02-17ER16362. Additionally, N. A. acknowledges support from the National Science Foundation Career Award Number CHE1555205.

VIII. DATA AVAILABILITY

The data that support the findings of this study are available from the corresponding author upon reasonable request.

- ¹R. Marcus and N. Sutin, *Biochimica et Biophysica Acta (BBA) - Reviews on Bioenergetics* **811**, 265 (1985).
- ²H. B. Gray and J. R. Winkler, *Annual Review of Biochemistry* **65**, 537 (1996), pMID: 8811189, <https://doi.org/10.1146/annurev.bi.65.070196.002541>.
- ³S. S. Skourtis, D. H. Waldeck, and D. N. Beratan, *Annual Review of Physical Chemistry* **61**, 461 (2010), pMID: 20192814, <https://doi.org/10.1146/annurev.physchem.012809.103436>.
- ⁴M. Azzouzi, J. Yan, T. Kirchartz, K. Liu, J. Wang, H. Wu, and J. Nelson, *Phys. Rev. X* **8**, 031055 (2018).
- ⁵D. R. Yarkony, *Chemical Reviews* **112**, 481 (2012), pMID: 22050109, <https://doi.org/10.1021/cr2001299>.
- ⁶S. Hammes-Schiffer and A. V. Soudackov, *The Journal of Physical Chemistry B* **112**, 14108 (2008), pMID: 18842015, <https://doi.org/10.1021/jp805876e>.
- ⁷R. A. Marcus, *The Journal of Chemical Physics* **24**, 966 (1956), <https://doi.org/10.1063/1.1742723>.
- ⁸P. G. Wolynes, *The Journal of Chemical Physics* **87**, 6559 (1987), <https://doi.org/10.1063/1.453440>.
- ⁹J. E. Lawrence and D. E. Manolopoulos, *The Journal of Chemical Physics* **148**, 102313 (2018), <https://doi.org/10.1063/1.5002894>.
- ¹⁰M. J. Thapa, W. Fang, and J. O. Richardson, *The Journal of Chemical Physics* **150**, 104107 (2019), <https://doi.org/10.1063/1.5081108>.
- ¹¹W. Fang, M. J. Thapa, and J. O. Richardson, *The Journal of Chemical Physics* **151**, 214101 (2019), <https://doi.org/10.1063/1.5131092>.
- ¹²W. Fang, R. A. Zarotiadis, and J. O. Richardson, *Phys. Chem. Chem. Phys.* **22**, 10687 (2020).
- ¹³Z. Tong, X. Gao, M. S. Cheung, B. D. Dunietz, E. Geva, and X. Sun, *The Journal of Chemical Physics* **153**, 044105 (2020), <https://doi.org/10.1063/5.0016160>.
- ¹⁴X. Sun, P. Zhang, Y. Lai, K. L. Williams, M. S. Cheung, B. D. Dunietz, and E. Geva, *The Journal of Physical Chemistry C* **122**, 11288 (2018), <https://doi.org/10.1021/acs.jpcc.8b02697>.
- ¹⁵J. E. Lawrence and D. E. Manolopoulos, *The Journal of Chemical Physics* **151**, 244109 (2019), <https://doi.org/10.1063/1.5138913>.
- ¹⁶E. R. Heller and J. O. Richardson, *The Journal of Chemical Physics* **152**, 034106 (2020), <https://doi.org/10.1063/1.5137823>.
- ¹⁷J. E. Lawrence and D. E. Manolopoulos, *The Journal of Chemical Physics* **152**, 204117 (2020), <https://doi.org/10.1063/5.0009109>.
- ¹⁸E. R. Heller and J. O. Richardson, *The Journal of Chemical Physics* **152**, 244117 (2020), <https://doi.org/10.1063/5.0013521>.
- ¹⁹J. Mattiat and J. O. Richardson, *The Journal of Chemical Physics* **148**, 102311 (2018), <https://doi.org/10.1063/1.5001116>.
- ²⁰J. E. Lawrence and D. E. Manolopoulos, *The Journal of Chemical Physics* **153**, 154113 (2020), <https://doi.org/10.1063/5.0022535>.
- ²¹J. E. Lawrence and D. E. Manolopoulos, *The Journal of Chemical Physics* **153**, 154114 (2020), <https://doi.org/10.1063/5.0022678>.
- ²²J. C. Tully, *The Journal of Chemical Physics* **93**, 1061 (1990), <https://doi.org/10.1063/1.459170>.
- ²³R. Kapral, *Annual Review of Physical Chemistry* **57**, 129 (2006), pMID: 16599807, <https://doi.org/10.1146/annurev.physchem.57.032905.104702>.
- ²⁴A. Jain and J. E. Subotnik, *The Journal of Chemical Physics* **143**, 134107 (2015), <https://aip.scitation.org/doi/pdf/10.1063/1.4930549>.
- ²⁵R. Crespo-Otero and M. Barbatti, *Chemical Reviews* **118**, 7026 (2018), pMID: 29767966, <https://doi.org/10.1021/acs.chemrev.7b00577>.
- ²⁶J. Cao and G. A. Voth, *The Journal of Chemical Physics* **106**, 1769 (1997), <https://doi.org/10.1063/1.474123>.
- ²⁷J. Cao, C. Minichino, and G. A. Voth, *The Journal of Chemical Physics* **103**, 1391 (1995), <https://doi.org/10.1063/1.469762>.
- ²⁸W. H. Miller and S. J. Cotton, *Faraday Discuss.* **195**, 9 (2016).
- ²⁹S. J. Cotton and W. H. Miller, *The Journal of Physical Chemistry A* **117**, 7190 (2013), pMID: 23432081, <https://doi.org/10.1021/jp401078u>.
- ³⁰J. O. Richardson, R. Bauer, and M. Thoss, *The Journal of Chemical Physics* **143**, 134115 (2015), <https://aip.scitation.org/doi/pdf/10.1063/1.4932361>.
- ³¹J. O. Richardson, *The Journal of Chemical Physics* **143**, 134116 (2015), <https://aip.scitation.org/doi/pdf/10.1063/1.4932362>.
- ³²M. K. Lee, P. Huo, and D. F. Coker, *Annual Review of Physical Chemistry* **67**, 639 (2016), pMID: 27090842, <https://doi.org/10.1146/annurev-physchem-040215-112252>.
- ³³N. Ananth, C. Venkataraman, and W. H. Miller, *The Journal of Chemical Physics* **127**, 084114 (2007), <https://doi.org/10.1063/1.2759932>.
- ³⁴M. S. Church, T. J. H. Hele, G. S. Ezra, and N. Ananth, *The Journal of Chemical Physics* **148**, 102326 (2018), <https://doi.org/10.1063/1.5005557>.
- ³⁵X. Liu and J. Liu, *The Journal of Chemical Physics* **148**, 102319 (2018), <https://doi.org/10.1063/1.5005059>.
- ³⁶J. Cao and G. A. Voth, *The Journal of Chemical Physics* **100**, 5106 (1994), <https://doi.org/10.1063/1.467176>.
- ³⁷S. Jang and G. A. Voth, *The Journal of Chemical Physics* **111**, 2371 (1999), <https://doi.org/10.1063/1.479515>.
- ³⁸I. R. Craig and D. E. Manolopoulos, *The Journal of Chemical Physics* **121**, 3368 (2004), <https://doi.org/10.1063/1.1777575>.
- ³⁹I. R. Craig and D. E. Manolopoulos, *The Journal of Chemical Physics* **122**, 084106 (2005), <https://doi.org/10.1063/1.1850093>.
- ⁴⁰J. E. Lawrence and D. E. Manolopoulos, *Faraday Discuss.* **221**, 9 (2020).
- ⁴¹I. S. Novikov, Y. V. Suleimanov, and A. V. Shapeev, *Phys. Chem. Chem. Phys.* **20**, 29503 (2018).
- ⁴²T. J. H. Hele and S. C. Althorpe, *The Journal of Chemical Physics* **138**, 084108 (2013), <https://doi.org/10.1063/1.4792697>.

- ⁴³S. C. Althorpe and T. J. H. Hele, *The Journal of Chemical Physics* **139**, 084115 (2013), <https://doi.org/10.1063/1.4819076>.
- ⁴⁴T. J. H. Hele and S. C. Althorpe, *The Journal of Chemical Physics* **144**, 174107 (2016), <https://doi.org/10.1063/1.4947589>.
- ⁴⁵S. Habershon, D. E. Manolopoulos, T. E. Markland, and T. F. Miller, *Annual Review of Physical Chemistry* **64**, 387 (2013), pMID: 23298242, <https://doi.org/10.1146/annurev-physchem-040412-110122>.
- ⁴⁶A. R. Menzeleev, N. Ananth, and T. F. Miller, *The Journal of Chemical Physics* **135**, 074106 (2011), <https://doi.org/10.1063/1.3624766>.
- ⁴⁷D. M. Wilkins, D. E. Manolopoulos, and L. X. Dang, *The Journal of Chemical Physics* **142**, 064509 (2015), <https://doi.org/10.1063/1.4907554>.
- ⁴⁸J. S. Kretchmer and T. F. Miller, *Inorganic Chemistry* **55**, 1022 (2016), pMID: 26440812, <https://doi.org/10.1021/acs.inorgchem.5b01821>.
- ⁴⁹Mean field RPMD has been used previously by many including D. E. Manolopoulos, T. F. Miller III, N. Ananth, J. C. Tully and I. R. Craig to evaluate nonadiabatic PI methods.
- ⁵⁰A. R. Menzeleev, F. Bell, and T. F. Miller, *The Journal of Chemical Physics* **140**, 064103 (2014), <https://doi.org/10.1063/1.4863919>.
- ⁵¹J. S. Kretchmer and T. F. Miller III, *Faraday Discuss.* **195**, 191 (2016).
- ⁵²J. S. Kretchmer, N. Boekelheide, J. J. Warren, J. R. Winkler, H. B. Gray, and T. F. Miller, *Proceedings of the National Academy of Sciences* **115**, 6129 (2018), <https://www.pnas.org/content/115/24/6129.full.pdf>.
- ⁵³J. O. Richardson and M. Thoss, *The Journal of Chemical Physics* **139**, 031102 (2013), <https://doi.org/10.1063/1.4816124>.
- ⁵⁴S. N. Chowdhury and P. Huo, *The Journal of Chemical Physics* **147**, 214109 (2017), <https://doi.org/10.1063/1.4995616>.
- ⁵⁵N. Ananth and T. F. Miller, *The Journal of Chemical Physics* **133**, 234103 (2010), <https://doi.org/10.1063/1.3511700>.
- ⁵⁶N. Ananth, *The Journal of Chemical Physics* **139**, 124102 (2013), <https://doi.org/10.1063/1.4821590>.
- ⁵⁷J. R. Duke and N. Ananth, *The Journal of Physical Chemistry Letters* **6**, 4219 (2015), pMID: 26722962, <https://doi.org/10.1021/acs.jpcclett.5b01957>.
- ⁵⁸S. Pierre, J. R. Duke, T. J. H. Hele, and N. Ananth, *The Journal of Chemical Physics* **147**, 234103 (2017), <https://doi.org/10.1063/1.4986517>.
- ⁵⁹J. Lu and Z. Zhou, *The Journal of Chemical Physics* **146**, 154110 (2017), <https://doi.org/10.1063/1.4981021>.
- ⁶⁰X. Tao, P. Shushkov, and T. F. Miller, *The Journal of Chemical Physics* **148**, 102327 (2018), <https://doi.org/10.1063/1.5005544>.
- ⁶¹X. Tao, P. Shushkov, and T. F. Miller, *The Journal of Physical Chemistry A* **123**, 3013 (2019), pMID: 30794746, <https://doi.org/10.1021/acs.jpca.9b00877>.
- ⁶²S. Ghosh, S. Giannini, K. Lively, and J. Blumberger, *Faraday Discuss.* **221**, 501 (2020).
- ⁶³T. J. H. Hele, “An electronically non-adiabatic generalization of ring polymer molecular dynamics,” (2013), arXiv:1308.3950 [physics.chem-ph].
- ⁶⁴J. R. Duke and N. Ananth, *Faraday Discuss.* **195**, 253 (2016).
- ⁶⁵D. Chandler, *Introduction to Modern Statistical Mechanics* (Oxford University Press, New York, 1987).
- ⁶⁶H. F. Trotter, *Proceedings of the American Mathematical Society* **10**, 545 (1959).
- ⁶⁷W. H. Miller, S. D. Schwartz, and J. W. Tromp, *The Journal of Chemical Physics* **79**, 4889 (1983), <https://doi.org/10.1063/1.445581>.
- ⁶⁸S. Ranya and N. Ananth, *The Journal of Chemical Physics* **152**, 114112 (2020), <https://doi.org/10.1063/1.5132807>.
- ⁶⁹R. A. Marcus and N. Sutin, *Biochim. Biophys. Acta* **811**, 265 (1985).
- ⁷⁰J. Ulstrup and J. Jortner, *J. Chem. Phys.* **63**, 4358 (1975).
- ⁷¹J. Ulstrup, *Charge Transfer Processes in Condensed Media* (Springer Verlag, Berlin, 1979).